Coherent alpha oscillations link current and future receptive fields during saccades

Sujaya Neupane[a,1], Daniel Guitton[a], and Christopher C. Pack[a]

[a]Department of Neurology & Neurosurgery, McGill University, Montreal, QC H3A2B4, Canada

Edited by Michael E. Goldberg, Columbia University College of Physicians, New York, NY, and approved June 6, 2017 (received for review January 31, 2017)

Oscillations are ubiquitous in the brain, and they can powerfully influence neural coding. In particular, when oscillations at distinct sites are coherent, they provide a means of gating the flow of neural signals between different cortical regions. Coherent oscillations also occur within individual brain regions, although the purpose of this coherence is not well understood. Here, we report that within a single brain region, coherent alpha oscillations link stimulus representations as they change in space and time. Specifically, in primate cortical area V4, alpha coherence links sites that encode the retinal location of a visual stimulus before and after a saccade. These coherence changes exhibit properties similar to those of receptive field remapping, a phenomenon in which individual neurons change their receptive fields according to the metrics of each saccade. In particular, alpha coherence, like remapping, is highly dependent on the saccade vector and the spatial arrangement of current and future receptive fields. Moreover, although visual stimulation plays a modulatory role, it is neither necessary nor sufficient to elicit alpha coherence. Indeed, a similar pattern of coherence is observed even when saccades are made in darkness. Together, these results show that the pattern of alpha coherence across the retinotopic map in V4 matches many of the properties of receptive field remapping. Thus, oscillatory coherence might play a role in constructing the stable representation of visual space that is an essential aspect of conscious perception.

communication through coherence | remapping | alpha frequency | saccades | V4

The brain's anatomical wiring can change in response to experience, on time scales ranging from minutes to years. At the same time, an organism's behavioral state can change far more quickly, necessitating a more flexible processing of sensory inputs. To change effective connectivity on these shorter time scales, the brain makes use of oscillatory coherence, which allows behaviorally relevant inputs to take precedence over others (1–6). For instance, previous work has shown that coherent gamma oscillations can facilitate the transmission of stimulus information between distinct brain regions during covert attention (3, 4).

Less is known about flexible communication within individual brain regions, but there is reason to suspect that it is useful as well (7–9). For instance, in sensory systems, space is represented in the form of maps that encode the location of individual stimuli. During natural sensory experience, stimuli can change position rapidly, requiring an updating of the corresponding sensory maps.

In most animals, the locations of visual stimuli are represented in retinotopic maps, which are commonly found in cortical and subcortical structures. During saccades, these maps are updated by a process known as receptive field remapping (10), whereby neurons transiently update their encoding of visual space to take account of the eye movement. Although the anatomical pathways that support remapping have been identified (11), the mechanisms that actually update receptive fields are poorly understood. However, given the rapid and flexible nature of remapping, it likely requires a transient change in effective connectivity (12).

Here, we have tested the hypothesis that saccadic remapping is associated with coherent local field potential (LFP) oscillations between distinct locations within a single retinotopic cortical map. We recorded simultaneously from many sites in primate cortical area V4, which has neurons that exhibit receptive field remapping (13, 14). By recording single-neuron and LFP signals in V4, we detected oscillatory coherence between recording sites with receptive fields representing the stimulus location before and after a saccade. Surprisingly, this coherence was strongest in the alpha frequency band and much weaker at gamma frequencies. These results suggest that oscillatory coherence in the alpha band serves to transfer sensory information within individual brain regions, thereby providing a means of updating spatial representations on short time scales.

Results

We recorded from area V4 in two macaque monkeys, using chronically implanted 96-channel multielectrode arrays. Each array provided access to multiple sites with receptive fields centered between 3° and 35° of retinal eccentricity for monkey N and between 3° and 16° for monkey P. We trained the animals to execute visually guided saccades and analyzed oscillatory coherence between the LFPs detected on pairs of electrodes.

While the animals performed the saccade task, we flashed probe stimuli that have been shown to elicit responses from V4 neurons and LFPs (14). The procedure is illustrated in Fig. 1*A* and in previous work (14, 15). On each trial, the animal acquired visual fixation (a 0.5° red square dot), after which we presented three visual probes (2° white squares) chosen randomly from within a large grid of possible locations (Fig. 1*A*). The probes were easily distinguishable from the saccade target based on color and location, because the saccade target location was consistent across trials within each day of recording. The first probe (P1), presented well before the saccade, allowed us to

Significance

Humans and other primates make frequent eye movements to inspect their surroundings. Consequently, stimuli that are stable in the environment are constantly changing position on the retina. One way for the brain to compensate for these changes is a mechanism called receptive field remapping, which allows individual neurons to encode the same object both before and after each saccade. Here, we provide a possible mechanism for remapping: Simultaneous recordings from cortical sites encoding the presaccadic and postsaccadic locations of a visual stimulus reveal coherent oscillations in the alpha frequency band. Because coherent oscillations are thought to play a role more generally in routing information within the brain, our findings provide a framework for understanding stable visual perception during eye movements.

Author contributions: S.N., D.G., and C.C.P. designed research; S.N. performed research; S.N. analyzed data; and S.N., D.G., and C.C.P. wrote the paper.

The authors declare no conflict of interest.

This article is a PNAS Direct Submission.

[1]To whom correspondence should be addressed. Email: sujaya.neupane@mail.mcgill.ca.

This article contains supporting information online at www.pnas.org/lookup/suppl/doi:10.1073/pnas.1701672114/-/DCSupplemental.

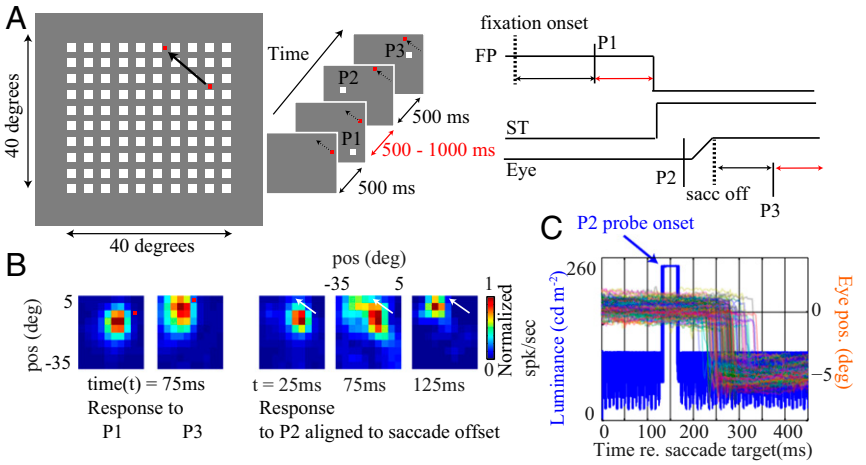

Fig. 1. Experimental design and example V4 neuron responses. (*A*, *Left*) Visual probes were chosen randomly from a grid of possibilities and then flashed at different positions and times relative to the onset of a visually guided saccade (black arrows). (*A*, *Right*) Three probes were presented on each trial, one long before the saccade (P1), one just before the saccade (P2), and one long after the saccade (P3). FP, fixation point; sacc, saccade; ST, saccade target. (*B*, *Left*) Responses of a typical V4 neuron, which had a fixation receptive field below and to the left of the fovea. (*B*, *Right*) For P2 probes, the receptive field remapped toward its postsaccadic location. deg, degrees; pos, position; spk, spikes. (*C*) Typical P2 probe luminance, as measured with a photodiode, shown in blue. Following probe offset on each trial, the saccade began, as indicated by the eye traces (colored lines). re., relative to.

characterize visual responses during steady fixation. The second probe (P2) was presented just before the saccade, when remapping mechanisms are active (10, 14); to avoid reafferent visual signals, we ensured that the P2 probe luminance had vanished before saccade onset on every trial (Fig. 1*C* and *Methods*). The third probe (P3) was presented long after the saccade, providing a measure of visual responses at the new fixation location. The animal was rewarded for following the fixation red dot by making a saccade and holding fixation until the dot moved back to the original fixation location.

Remapping of Single-Neuron Receptive Fields in V4. We have previously shown that most V4 neurons exhibit receptive field remapping under the experimental conditions used here (14, 16). For completeness, a typical example from the current dataset is shown in Fig. 1*B* (*Left*): The panels show the receptive field of an example V4 neuron; for both P1 and P3 probes, responses were strongest at a position to the left and just below fixation (red dot). In contrast, for P2 probes flashed just before a left-upward saccade (Fig. 1*B*, *Right*), the receptive field was displaced away from both the saccade target and the P1 receptive field, toward the P3 receptive field location. These remapped responses were most apparent starting about 100 ms after the completion of the saccade (14) (Fig. 1*B*); Fig. S1*A* shows similar receptive field shifts for the population of 32 neurons recorded simultaneously during this experiment.

Coherence of Oscillations During Receptive Field Remapping. To examine a possible oscillatory basis for this remapping, we recorded simultaneously from sites that encoded the presaccadic and postsaccadic spatial locations of V4 receptive fields. We refer to these locations as the current and future receptive fields. Based on the retinotopic layout of each array, we chose saccade vectors that maximized the coverage of current and future receptive fields in each animal (horizontal and vertical in monkey N, oblique in monkey P; Fig. S1*B*). We note that these experiments were not designed to study the perisaccadic convergence of V4 receptive fields toward the saccade target, a phenomenon that has different properties from the remapping we are studying here (13, 14).

Fig. 2*A* shows the layout for the array in monkey N, with each blue dot indicating the center of the receptive field measured at a single electrode. We used the LFPs to define receptive field locations, based on previous observations that LFP retinotopy in V4 closely matches the retinotopy of spiking activity (17). For a 10° leftward saccade, a neuron with a receptive field centered at the blue dot (Fig. 2*A*) would have a corresponding future field 10° to the left. We hypothesized that LFP oscillations for sites in the vicinity of the future field (light red circle in Fig. 2*A*) would have oscillations that were coherent with sites encoding the current field location around the time that remapping was occurring in the single-unit activity. We further hypothesized that coherence between the current field and control sites distant from the future field (gray circle in Fig. 2*A*) would be far weaker.

Fig. 2*B* shows the raw voltage traces for LFP signals recorded at the current field location and one future field location (dark red circle in Fig. 2*A*), as well as an electrode encoding a control location (small black circle in Fig. 2*A*) displaced vertically from both current and future field sites. These traces correspond to the average LFP signal relative to the offset of each leftward saccade. For these analyses, we considered only those trials in which a P2 probe was flashed near the future field location, which is when remapping occurs in single neurons (14) (Fig. S1*A*).

As found previously (18, 19), LFP signals were affected strongly by the saccade, with changes in amplitude and coherence being apparent in the raw traces. Importantly, the LFP signals at the current (blue) and future field (red) locations (Fig. 2*B*) became more similar in the period immediately following the saccade ($P = 0.1$, Mann–Whitney U test for average LFP values between 50 ms and 200 ms; $n = 128$ trials). At the same time, the LFP responses at the current field and control site (black circle in Fig. 2*A*) diverged ($P < 0.01$, Mann–Whitney U test for average LFP values between 50 ms and 150 ms; $n = 128$ trials).

To quantify these effects for the example sites, we computed a standard metric of oscillatory coherence (20), and plotted it across time and frequencies. Fig. 2*C* shows the coherence spectrogram computed in a sliding 200-ms time window (*Methods*). Consistent with the raw traces, the current-future field pairs (Fig. 2*C*, *Left*) showed an increase in coherence that started around the time of the eye movement and persisted for some time after the saccade was complete. This increase was significant for frequencies below 15 Hz ($P = 0.002$, Mann–Whitney U test). By comparison, coherence between the current field and control site

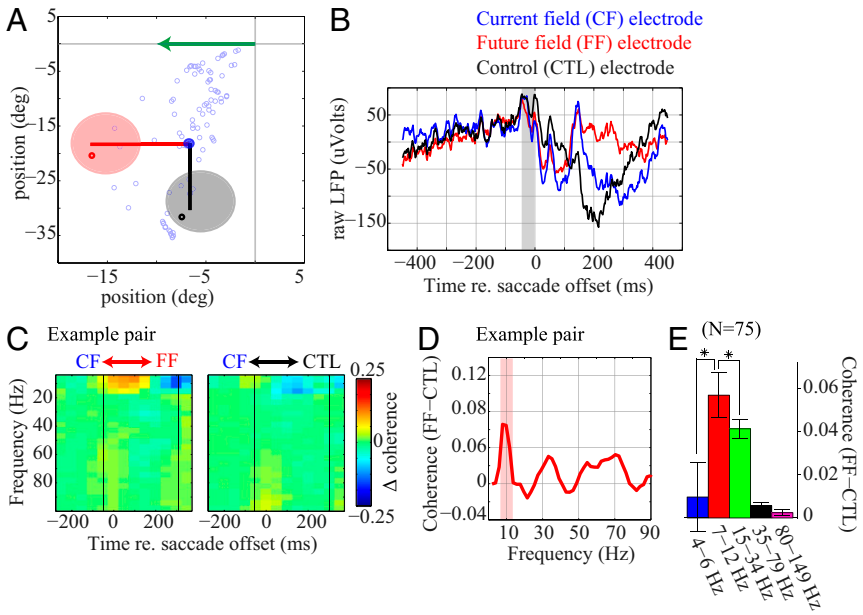

Fig. 2. Examples of perisaccadic changes in oscillatory coherence. (*A*) Retinotopic layout of electrode sites in monkey N. Each open circle corresponds to the center of the LFP receptive field measured on one electrode. For a leftward saccade (green arrow), a current field electrode with a receptive field located at the solid blue dot would show remapping in the leftward direction. Electrodes with receptive fields near the future field center (light red circle) were considered as future field pairs. Electrodes with receptive fields far from the current and future field centers (gray circle) were considered as control pairs. The control location was at the same distance from the current field as the future field. Note that the gray and light red circles are not drawn to scale. (*B*) Raw LFP traces for example current (blue), future (red), and control (black) electrode sites, aligned to saccade offset. The shaded gray window indicates typical saccade duration. (*C*) Coherence spectrograms for the current-future field pair (*Left*) and the current field-control pair (*Right*). The vertical lines indicate the analysis time window for the postsaccadic epoch, which is normalized by the baseline epoch (−450 to −100 ms relative to saccade offset) (*D*) Perisaccadic differences in coherence across frequencies between the current-future field pair and current-control field pair. (*E*) Mean coherence changes for 75 current-future field pairs relative to current-control field pairs, for standard frequency bands. Asterisks indicate statistically significant differences between current-future field and current field-control coherence levels ($P < 0.05$, *t* test; $n = 75$).

(Fig. 2*C*, *Right*) increased very little at any frequency, including those frequencies below 15 Hz ($P = 0.61$, Mann–Whitney *U* test). Thus, for this example, the saccade led to increased low-frequency coherence between the current and future field sites during a time period confined to the immediate postsaccadic period. Similar results were found for the population of 75 electrode pairs (Fig. S2*A*).

Having localized the coherence changes in time and space, we next attempted to determine which LFP frequencies showed the strongest coherence changes between current and future field sites. To increase our resolution at low frequencies, we used a larger time window (350 ms; *Methods*) centered on the postsaccadic period. Fig. 2*D* shows the difference between current-control field coherence and current-future field coherence for the example sites shown in Fig. 2*C*; there was a peak near 10 Hz, with clear coherence increases in the range of 7–12 Hz ($P < 0.05$, Mann–Whitney *U* test). The full power spectra for the individual electrode pairs are shown in Fig. S2*B*.

To assess the generality of this result, we calculated changes in coherence during the same perisaccadic time period in standard frequency bands: theta (4–6 Hz), alpha (7–12 Hz), beta (15–34 Hz), gamma (35–80 Hz), and high gamma (80–150 Hz) for 75 additional current-future field pairs. As in the example recordings, the alpha band consistently showed higher increases in relative coherence around the time of a 10° leftward saccade ($P << 0.0001$, right-tailed two-sample *t* test; $n = 75$; Fig. 2*E*).

The results for other saccade vectors (Figs. S3*A* and S4*B*) show that perisaccadic alpha coherence was similarly greater for control-future field pairs than for current field-control pairs. This trend was not consistently found across saccade vectors for any other frequency band (Fig. S3*A*, *Right*), and it was particularly evident in the alpha band when we recalculated coherence changes in a 200-ms time window (Fig. S3*B*). In this case, there was a strong increase in alpha coherence for all saccade vectors, with little consistent change in higher frequencies. Thus, perisaccadic changes in current-future field alpha coherence were robust to different analysis time windows and saccade vectors. Because these coherence changes were specific to the current-future field electrode pairs, they could not be attributed to a global synchronization of LFP signals across V4 (17) or to nonspecific visual landmarks. We therefore focused our remaining analyses on this frequency band.

Alpha Coherence Depends on the Saccade Vector. To the extent that alpha coherence is associated with remapping, its retinotopic pattern should change with the direction and amplitude of the saccade. To test this prediction, we exploited the arrangement of the electrode array in monkey N (Fig. 2*A*) to define horizontal and vertical pairings of electrodes. We then measured coherence changes during performance of horizontal and vertical saccades. Under this geometry, the same electrode pairs could serve as current-future field pairs or as current field-control pairs, depending on the saccade vector. For example, during performance of the 10° leftward saccade (Fig. 2), we were able to define 75 current-future field pairs, and these current-future field pairs are shown as the red lines in Fig. 3*A*. The black lines in Fig. 3*A* show 75 additional pairs of electrodes with receptive field centers displaced vertically by about 20°; these additional pairs served as the current field-control pairs. However, during performance of a 20° vertical saccade, these pairs of electrodes took on the opposite labels (Fig. 3*C*).

Fig. 3*B* (red line) shows the mean change in alpha coherence for each current-future field electrode pair around the time of the 10° leftward saccade. As in Fig. 2, there was an increase in coherence starting just before saccade onset and continuing for

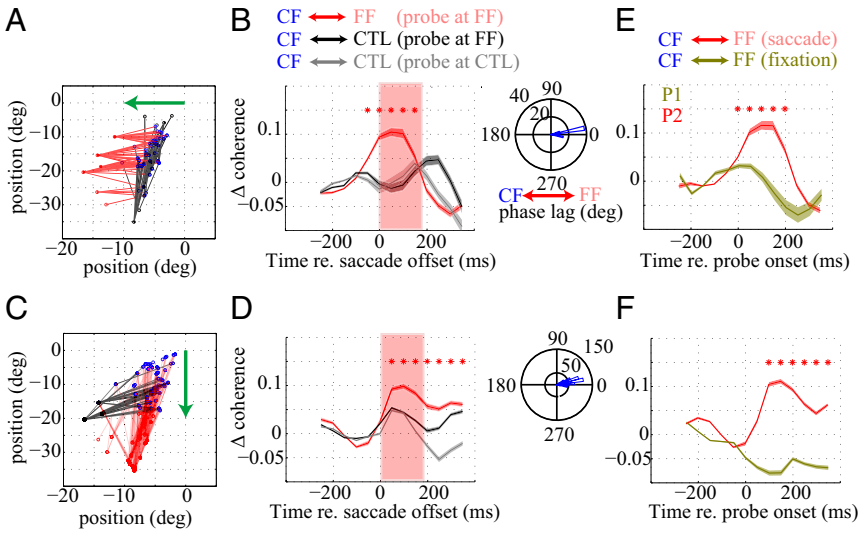

Fig. 3. Dependence of alpha coherence on the saccade vector. (*A*) Current-future field (red) and current field-control (black) electrode pairs during performance of a 10° leftward saccade by monkey N. (*B*, *Left*) Mean coherence change, relative to the presaccadic baseline, for current-future field pairs (red), for current field-control pairs (black) when probes were flashed in the future field, and for current field-control pairs when probes were flashed in control field sites (gray). The shaded region represents the SEM, and asterisks indicate statistically significant differences between current-future field pairs and current field-control pairs ($P < 0.05$, paired t test; $n = 75$). Here, as elsewhere, time is aligned to saccade offset, and each time point corresponds to the center of a 200-ms bin. (*B*, *Right*) Distributions of alpha-phase differences between the future and current field electrode sites for the different saccade vectors. The radius represents the number of current-future field pairs, and the angles represent the phase lag of alpha oscillation at the current field relative to the phase lag of alpha oscillation at the future field. (*C* and *D*) Same as in *A* and *B*, but for 20° vertical saccades ($P < 0.05$, paired t test; $n = 256$). (*E* and *F*) Mean coherence change during fixation with all of the other conditions (receptive field-FF pairs and probe location) fixed.

nearly 150 ms after the completion of the saccade. Mean coherence between current field and control sites was significantly weaker (black line in Fig. 3*B*; $P < 0.0001$, paired t test; $n = 75$). For this saccade vector, there was an increase in current-control field coherence at later time points (Fig. 3*B*), but this increase was not seen for other saccade vectors (Fig. 3*B* and Fig. S5 *I* and *J*).

For the 20° vertical saccade, coherence was again stronger for current-future field pairs, which were now separated vertically (red line in Fig. 3*D*), and weaker for current-control pairs, which were now separated horizontally (black line in Fig. 3*D*; $P < 0.0001$, paired t test; $n = 256$). For both saccade vectors, the increase in coherence peaked around 100 ms after the saccade offset. Similar results were obtained for monkey P (Fig. S5 *I* and *J*). By comparison, current-future field coherence in the beta and gamma bands did not show consistent perisaccadic changes at the same time points (19) (Fig. S6). We note that for some saccades, there was also an increase in beta coherence around the time of the saccade (before remapping); this increase in beta coherence is a signature of the postsaccadic traveling waves that we have reported previously (19). We return to this point later (*Discussion*).

To ensure that the increase in the current-future field coherence pattern was not caused purely by visual stimulation, we performed two additional control analyses. First, we computed alpha coherence for the same stimuli and the same current-future field pairs during steady fixation in response to P1 probes. In this case, there was little change in coherence (Fig. 3 *E* and *F*), indicating that the saccade was necessary for the coherence change. To further ensure that coherence was not triggered by visual stimulation, we computed current field-control coherence for trials in which the probes were flashed at the control sites (gray traces in Fig. 3 *B* and *D*). For both saccade vectors, the coherence between current field-control pairs was significantly weaker than between future field-control pairs when probes were flashed in the future field ($P < 0.0001$, paired t test). Thus, the increase in alpha coherence was not merely a consequence of the presentation of the stimulus probe; indeed, as we show below (Fig. 4*C*), some increase in current-future field coherence could be observed when no probes were presented at all.

Alpha-Phase Relationships Could Support Remapping. Enhanced coherence could serve to transfer visual information from the future field site to the current field site (21), as suggested by some theories of remapping (12, 22–24). To test this idea, we calculated the phase differences between perisaccadic alpha oscillations at the two sites. The results for both saccade directions (Fig. 3 *B* and *D*, *Right*) show that the current field phase consistently lagged the future field phase (null hypothesis: mean slope = 0°; $P < 0.05$, one-sample test; $n = 83$ for horizontal and $n = 509$ for vertical), suggesting that information flowed from the future to the current field (5, 7). The lag was, on average, 9.7 ± 1.1°, which translates into 2.7 ms. Results were similar for monkey P (Fig. S4*A*). We note also that the change in alpha coherence generally began significantly earlier than the latency of remapping responses in single neurons ($P << 0.0001$, Mann–Whitney U test; Fig. S7 *A* and *B*).

Perisaccadic Alpha Coherence Is Approximately Constant Across the Visual Field. Alpha oscillations are often associated with attention (25, 26), and so an alternative way to think about these results is that they are a side effect of spatial attention directed toward the fixation point or toward the saccade target. This hypothesis would predict a significant variation of alpha coherence across retinotopic space. In contrast, receptive field remapping in single neurons appears to be constant across the visual field (14, 27, 28). Our data were more consistent with the properties of remapping: Perisaccadic alpha coherence was largely independent of both future field (linear regression: $r^2 = 0.000016$, $P = 0.92$) and current field (linear regression: $r^2 = 0.000036$, $P = 0.17$) eccentricity (alpha coherence for all electrode pairs sorted by eccentricity is illustrated in Fig. S5 *B*, *D*, *F*, and *H*). Alpha coherence was also largely independent of the overlap between

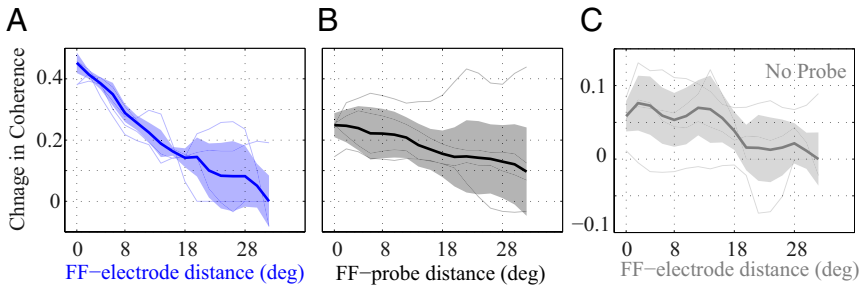

Fig. 4. Dependence of alpha coherence on the electrode separation and probe position. (*A*) Change in alpha coherence as a function of Pythagorean distance between the future field center and the receptive field centers of other electrodes. The FF electrode distance indicates the distance between the FF center of a reference electrode and the receptive field center of all of the other electrodes. Thin lines indicate individual saccade vectors, and the thick line indicates the average across saccade vectors. The error shade represents the variance across the four saccade vector traces. (*B*) Change in alpha coherence as a function of distance between the future field center and the position of the P2 probe. (*C*) Change in alpha coherence as a function of electrode separation when no probe is presented; note that the *y* axis is scaled relative to the preceding panels.

the current and future receptive fields (*Methods* and Fig. S7*C*; $P > 0.12$).

Alpha Coherence Is Modulated by Receptive Field Separation and Visual Stimulation. The results thus far show that alpha coherence is strongest between electrodes with fields that are separated by the saccade vector (current-future field pairs) and when the P2 probe is near the future field (Fig. 3). In other words, alpha coherence depends on receptive field separation and visual stimulation, but it is not clear which factor is more important. To quantify the relative influence of these two factors, we examined alpha coherence for all possible pairs of electrodes and all P2 probe positions, using singular value decomposition (SVD) (*Methods* and Fig. S8*A*).

Fig. 4*A* shows the median alpha coherence between each current field electrode and all other electrodes on the array, independent of P2 probe location. In this plot, the receptive field separation is described with respect to the future field, so that current-future field pairs would occupy position zero on the *x* axis. Coherence between the current field electrode and electrodes with receptive fields located farther from the future field is shown at greater values along the *x* axis. As expected, coherence decreases steadily as the position of each receptive field center deviates from the future field location. This finding is true for each saccade vector across both monkeys (thin blue lines in Fig. 4*A*; $P < 0.05$, Spearman's rank-order correlation) and for the average of all saccade vectors (thick blue line in Fig. 4*A*).

Fig. 4*B* shows the perisaccadic alpha coherence between pairs of electrodes as a function of distance between the P2 probe and the future field center. This plot combines information from all electrode pairs. Again, alpha coherence declines with distance, and this trend is apparent for each saccade vector (thin gray lines in Fig. 4*B*; $P < 0.05$, Spearman's rank-order correlation). The exception is the vertical saccade case, for which the future field eccentricity was very large (>30°); consequently, we were unable to present probes far outside the future field. Overall, the sensitivity of alpha coherence to probe position is weaker than the sensitivity to electrode separation.

Across all experimental conditions, the receptive field separation (in spatial coordinates) and the probe position accounted very well for the complete pattern of alpha coherence (Fig. S8*B*). Our SVD analysis revealed that, depending on the saccade vector, these two factors captured between 60% and 91% of the variance in alpha coherence across conditions. The remaining patterns of alpha coherence were unstructured, being indistinguishable from random permutations of the observed coherence values (*Methods*; permutation test).

These results show that alpha coherence is modulated by both electrode separation and probe position, with the latter being less precise. Interestingly, the dependence of alpha coherence on electrode separation persisted even when no probe was presented (Fig. 4*C*; $P < 0.05$, Spearman's rank-order correlation). Thus, a visual probe was neither sufficient (Fig. 3) nor necessary (Fig. 4*C*) to trigger a change in alpha coherence. This result suggests that saccades automatically impose alpha-band coherence between the appropriate sites in V4 by virtue of a corollary discharge signal that represents eye displacement or position, as has been found in other parts of the visual cortex (29). This coherence is then magnified by the presentation of a visual stimulus at the appropriate position.

Discussion

We have shown that alpha coherence provides a basis for flexible communication within a single brain area. Specifically, during saccades, alpha coherence links sites that would be expected to share a common stimulus representation. Overall, the observed pattern of coherence has properties similar to the properties of single-neuron remapping, being strongest after the completion of the saccade (Fig. 2), specific to the saccade vector (Fig. 3), and modulated by visual stimulation (Fig. 4).

Oscillatory Coherence and Remapping. Our results are generally consistent with the idea that coherent oscillations facilitate the binding of the different features that make up a single object (9). Previous work on this topic has emphasized the role of gamma (~40 Hz) oscillations in linking these features across retinotopic space (9). The challenge of integrating information across saccades could be viewed similarly: With each saccade, a single object will appear at different retinal locations at different points in time. Remapping provides a mechanism by which individual neurons can integrate these different views of the same object (30, 31); in this sense, it entails a spatiotemporal binding of visual information. Our results suggest that the brain uses alpha oscillations to carry out this operation.

In addition to alpha coherence, our results showed increased beta coherence for some saccade vectors (Fig. 2 and Fig. S6). This beta coherence reflects postsaccadic traveling waves (19), which are unlikely to be related to remapping for several reasons. First, the traveling waves end before remapping starts (Fig. S6). Second, they are found only for saccades toward the receptive fields, whereas remapping is relatively independent of saccade direction (14, 16, 27). Finally, they occur for visual stimulus conditions in which no remapping is observed (19, 25).

Regardless of the specific frequencies involved, our results provide a connection between LFP oscillations and "future field" or "forward" remapping (16). Specifically, our experiments are generally consistent with previous observations of memory remapping, a type of forward remapping that is apparent well

after the saccade is complete (14, 32, 33). Neurons in oculomotor areas also exhibit "predictive" forward remapping, in which the remapped responses can be detected even before the saccade (10). Because we usually presented P2 probes just before saccade onset, our data do not address potential predictive remapping in V4.

Previous studies on this topic in V4 (13, 14) and frontal eye fields (15) have characterized yet another type of remapping, known as "convergent" remapping, in which receptive fields shift toward the location of the saccade target. Convergent remapping is strongest for saccades directed close to the receptive field centers (13), and it can be modeled simply as a localized modulation of the gain of visual responses (34), without the need for changes in oscillatory coherence. For this reason, we designed our experiments specifically to probe forward remapping, although it would be interesting to determine whether convergent remapping is also associated with changes in oscillatory coherence.

Meaning of LFP Coherence. The question naturally arises as to whether oscillatory coherence is a cause or a consequence of remapping. Theoretical models have shown how networks of laterally connected neurons can implement remapping (12, 22–24), and coherent alpha oscillations might emerge as a side effect of these operations. In that case, alpha coherence would not be necessary for remapping, although it could still facilitate the transmission of the remapped signals to other brain areas (21).

An alternative interpretation is that the brain uses oscillatory coherence to generate remapping in single neurons. In this scenario, the temporal alignment of oscillations at the current and future field sites would permit the transmission of stimulus information within V4 (3, 21). Such coherence might be imposed by subcortical areas (1) or by cortical areas with nonretinal spatial representations (35). Our results on the relative latencies of alpha coherence and single-neuron remapping (Fig. 3 and Fig. S7 *A* and *B*) are consistent with this idea, as are the phase relationships between alpha oscillations at the current and future field sites (Fig. 3 *B* and *D* and Fig. S4*A*). This latter result suggests that communication between the two locations could occur on time scales considerably shorter than the period of an alpha oscillation.

Finally, we note that for monkey N, there were very few channels (typically 11 of 96) that exhibited any single-neuron activity, suggesting that strong spiking activity is not necessary for alpha coherence. This idea is consistent with the idea that alpha coherence is imposed by oscillations originating in other brain structures, and this hypothesis could be tested with reversible inactivation of thalamic structures known to synchronize with the cortex in alpha bands (1, 36). The pulvinar might be a particularly fruitful target, given its role in synchronizing intracortical processing (1) and in relaying saccade-related signals to the visual cortex (37). This structure also appears to be involved in the allocation of attention, and so it would be interesting to examine alpha coherence during a task in which attention affects remapping (38). Functionally, an external source for alpha modulation fits with previous work indicating a role for alpha coherence in regulating top-down interareal communication (39, 40). These studies point specifically to a role for alpha coherence in anticipating the appearance of future stimuli (41, 42) and in short-term memory (40). Coherent alpha oscillations are particularly apparent in thalamocortical circuits (1, 36), which are crucial for remapping (11). These pathways could thus support the hypothesized role of "memory remapping" in maintaining a representation of stimuli that have disappeared from view (32, 33), as is necessary to construct a stable representation of sensory space.

Methods

Electrophysiological Recordings. Two monkeys (*Macaca fascicularis*, both female) were subjects in the experiments. The recording methods have been described previously (14, 17, 19). Briefly, a sterile surgical procedure was carried out to implant a head-post, after which monkeys were trained to make visually guided saccades for liquid rewards. A chronic 10 × 10-microelectrode Utah array (400-μm electrode spacing; Blackrock Microsystems) was then implanted into area V4. All aspects of the experiments were approved by the Animal Care Committee of the Montreal Neurological Institute and were conducted in compliance with regulations established by the Canadian Council of Animal Care.

Signal Acquisition and Preprocessing. Wideband signals were recorded using a data acquisition system (Plexon Multichannel Acquisition Processor System) with custom modification of the preamplifier as described previously (43). Action potential waveforms were removed from the wideband signal (43), which was then bandpass-filtered (0.2–150 Hz) to provide the LFPs.

Experimental Paradigm. Visual stimuli were presented either on an LG OLED (model 55EC9300) or Toshiba LED (model 65l350U) screen, each with a refresh rate of 100 Hz. These devices were chosen for their extremely high temporal precision, as illustrated in Fig. 1*C*, which plots superimposed traces of 120 example trials in which a probe was displayed on the OLED screen before saccade onset. The response timing was highly repeatable across days and virtually identical for the LED screen. Both screens covered a viewing area of 80° at a distance of 78 cm. All visual stimuli were white square probes [luminance = 260 cd/m^2 (OLED) and 158 cd/m^2 (LED)] presented for 30 ms on a dim gray background [luminance = 26 cd/m^2 (OLED) and 13 cd/m^2 (LED)].

Each trial started with the animal fixating on a red dot (0.5° in diameter). If fixation deviated from the target by more than 2.5°, the trial was aborted. After 500 ms of fixation, a visual probe (P1) was flashed at a randomly chosen location from 100 different locations arranged in a 10 × 10 grid in the lower left quadrant of the visual field (Fig. 1*A*). The size and location of the grid were chosen to span the retinal eccentricities of all of the simultaneously recorded receptive fields. Each probe was square in shape, 2° in width, and spaced at 4° (center-to-center) from its neighbors in the horizontal and vertical dimensions. After a variable delay of 500–1,000 ms, the fixation point jumped to a new target. A second probe (P2) was flashed after the appearance of the saccade target, with the timing chosen according to the distribution of saccade latencies for each monkey (100 ms after the saccade target appearance for monkey N and 130 ms for monkey P). The median P2 offset time relative to the saccade onset was −39 ms for monkey N and −55 ms for monkey P. To ensure that P2 flashes were completely off before saccade onset, luminance decay on the screen was measured with a photodiode on each trial (Fig. 1*C*). The rise and fall times of probe onset and offset for both monitors were less than 1 ms, as measured by a photodiode (Fig. S1*C*). Any trial in which the saccade started less than 40 ms after the probe offset was discarded. After the saccade, the monkey was required to fixate for another 500 ms, after which a third probe (P3) was flashed. After another 500–1,000 ms of fixation, the trial ended with a liquid reward to the monkey. We also randomly interleaved trials in which no probes were flashed. Trials were repeated such that there were at least 10–15 trials per probe location for each type of probe (P1, P2, and P3). Eye position was monitored using an IR eye tracker (Eyelink; SR Research).

Data Analyses.

Eye movements. Saccade onset was defined as the time when the eye trace left the fixation window and crossed a velocity threshold of 200°/s. Saccade offset was the time when eye trace decreased its velocity below 200°/s. Any trial in which the eye was not within the saccade window or the fixation window (±2.5°) was discarded. We also discarded trials that contained blinks or double-step or catch-up saccades.

LFP receptive field center estimation. We used a method defined previously (17) to extract the retinotopic component of the LFP. Briefly, a generative model was fitted to the data to capture the retinotopic and global components of LFP responses to stimuli flashed at multiple locations on the screen. The global component was removed from the signal to obtain the retinotopic component, which matched the retinotopy obtained with spiking activity. This procedure yielded Gaussian receptive fields, the centers of which corresponded to the receptive field centers used throughout the study. For the analysis reported in Fig. S7*C*, the overlap between each pair of receptive fields was estimated with the cumulative trapezoidal method in MATLAB (MathWorks).

Coherence analysis. For the analyses shown in Figs. 2 and 3, we first defined the center of each electrode's receptive field in retinal coordinates (Fig. S1*B*). We considered each electrode as a potential current field site; the center of the future field was then equal to the current receptive field center shifted by the saccade vector. On this basis, we defined the corresponding future field sites as all those electrodes with receptive field centers within 4° of the future field center. The number of current-future field pairs for a given

current receptive field site ranged from none to 19. The current field-control sites were chosen analogously, except that the direction of the control site was perpendicular to the saccade vector. We analyzed only trials in which the P2 probe was within 4° of the future field or control field center.

Coherence was computed between all of the pairs of electrodes using a multitaper method (chronux.org) with five orthogonal tapers and a time-bandwidth product of 3 (corresponding to a spectral width of 15 Hz for a 200-ms time window) for LFPs sampled at 500 Hz. In all cases, the LFP time series was aligned to saccade offset, and the temporal profile of coherence was generated by windowing the 800-ms LFP time series in a 200-ms window and sliding the window in steps of 50 ms. The average presaccadic coherence (−250 to −50 ms) was used for baseline normalization. To achieve a higher resolution of coherence at frequencies below 15 Hz, we divided the LFP time series into two nonoverlapping windows with a length of 350 ms (with time-bandwidth product of 2 corresponding to a spectral width of ∼5 Hz), one representing the presaccadic baseline epoch (−450 to −100 ms) and the other representing the perisaccadic epoch (−50 to 300 ms). The same windowing scheme was used to compute the phase distribution of the alpha coherence in three frequency bins (8 Hz, 10 Hz, and 12 Hz) pooled together. To quantify the mean phase, we pooled only those pairs with tuned phase distributions ($P < 0.05$, Rayleigh nonuniformity test). The distribution of mean phase was used to quantify the lag between receptive field and future field sites. The latency of coherence (Fig. S7*A*) was calculated as the time when the coherence between a given receptive field-future field pair surpassed 3 SDs above the average presaccadic baseline computed across all of the receptive field-future field pairs for the corresponding saccade vectors.

SVD. To test for the relative importance of probe position and receptive field separation to alpha coherence, we considered each electrode's receptive field as a current field site (Fig. S8*A*). We determined its future field location, based on the corresponding saccade vector. We then chose another electrode and calculated the distance between its receptive field center and the future field center. Finally, we calculated the alpha coherence between these two electrodes for each P2 probe location. We performed this operation for each electrode that could be paired with the current field electrode. Combining these measurements across all current field electrodes provided a 2D matrix of alpha coherence as a function of two distances: (*i*) receptive field center relative to the future field center, and (*ii*) probe location relative to the future field center (Fig. S8*B*).

To extract the contribution of each factor to alpha coherence, we performed an SVD of the alpha coherence matrix for each saccade vector. The first singular vectors are plotted in Fig. 4 *A* and *B*. To test for the statistical significance of these singular values, we shuffled each matrix 100 times and recalculated the SVD. This procedure generated a baseline distribution of singular values, allowing us to define significance as 2 SDs above the mean of this distribution. By this measure, only the first singular value was significant for each saccade vector, indicating that the effects of electrode distance and probe distance were separable. Therefore, we were able to study the effect of receptive field distance and probe distance on coherence independently.

Estimation of single-neuron receptive fields. Receptive fields were estimated as described previously (14). Briefly, spike times were assigned to 25-ms bins spanning the period between 350 ms before and after the saccade offset. At each time point, the spiking activity across probe locations was smoothed and then interpolated, after which each spatial position was weighted by its corresponding firing rate. The weighted probe locations were summed and divided by the total firing rate to obtain the center of gravity of the receptive field responses in Cartesian coordinates.

All of the data will be available upon request.

ACKNOWLEDGMENTS. We thank Julie Coursol and Cathy Hunt for outstanding animal care and Drs. Fernando Churaund and Julio Martinez-Trujillo for help with surgical procedures. This work was supported by Canadian Institutes of Health Research (CIHR) Grant PJT-148488 and Natural Sciences and Engineering Research Council (NSERC) Grant 341534-12 (to C.C.P.), CIHR Grant MOP-9222 (to D.G.), and NSERC Doctoral Award PGSD2-459756-2014 and Ann and Richard Sievers Award 2016 (to S.N.).

1. Saalmann YB, Pinsk MA, Wang L, Li X, Kastner S (2012) The pulvinar regulates information transmission between cortical areas based on attention demands. *Science* 337:753–756.
2. Womelsdorf T, et al. (2007) Modulation of neuronal interactions through neuronal synchronization. *Science* 316:1609–1612.
3. Bosman CA, et al. (2012) Attentional stimulus selection through selective synchronization between monkey visual areas. *Neuron* 75:875–888.
4. Grothe I, Neitzel SD, Mandon S, Kreiter AK (2012) Switching neuronal inputs by differential modulations of gamma-band phase-coherence. *J Neurosci* 32:16172–16180.
5. Gregoriou GG, Gotts SJ, Zhou H, Desimone R (2009) High-frequency, long-range coupling between prefrontal and visual cortex during attention. *Science* 324:1207–1210.
6. Buschman TJ, Miller EK (2007) Top-down versus bottom-up control of attention in the prefrontal and posterior parietal cortices. *Science* 315:1860–1862.
7. Besserve M, Lowe SC, Logothetis NK, Schölkopf B, Panzeri S (2015) Shifts of gamma phase across primary visual cortical sites reflect dynamic stimulus-modulated information transfer. *PLoS Biol* 13:e1002257.
8. Colgin LL, et al. (2009) Frequency of gamma oscillations routes flow of information in the hippocampus. *Nature* 462:353–357.
9. Gray CM, König P, Engel AK, Singer W (1989) Oscillatory responses in cat visual cortex exhibit inter-columnar synchronization which reflects global stimulus properties. *Nature* 338:334–337.
10. Duhamel JR, Colby CL, Goldberg ME (1992) The updating of the representation of visual space in parietal cortex by intended eye movements. *Science* 255:90–92.
11. Sommer MA, Wurtz RH (2006) Influence of the thalamus on spatial visual processing in frontal cortex. *Nature* 444:374–377.
12. Cavanagh P, Hunt AR, Afraz A, Rolfs M (2010) Visual stability based on remapping of attention pointers. *Trends Cogn Sci* 14:147–153.
13. Tolias AS, et al. (2001) Eye movements modulate visual receptive fields of V4 neurons. *Neuron* 29:757–767.
14. Neupane S, Guitton D, Pack CC (2016) Two distinct types of remapping in primate cortical area V4. *Nat Commun* 7:10402.
15. Zirnsak M, Steinmetz NA, Noudoost B, Xu KZ, Moore T (2014) Visual space is compressed in prefrontal cortex before eye movements. *Nature* 507:504–507.
16. Neupane S, Guitton D, Pack CC (2016) Dissociation of forward and convergent remapping in primate visual cortex. *Curr Biol* 26:R491–R492.
17. Mineault PJ, Zanos TP, Pack CC (2013) Local field potentials reflect multiple spatial scales in V4. *Front Comput Neurosci* 7:21.
18. Ito J, Maldonado P, Singer W, Grün S (2011) Saccade-related modulations of neuronal excitability support synchrony of visually elicited spikes. *Cereb Cortex* 21:2482–2497.
19. Zanos TP, Mineault PJ, Nasiotis KT, Guitton D, Pack CC (2015) A sensorimotor role for traveling waves in primate visual cortex. *Neuron* 85:615–627.
20. Mitra PP, Pesaran B (1999) Analysis of dynamic brain imaging data. *Biophys J* 76:691–708.
21. Fries P (2015) Rhythms for cognition: Communication through coherence. *Neuron* 88:220–235.
22. Keith GP, Blohm G, Crawford JD (2010) Influence of saccade efference copy on the spatiotemporal properties of remapping: A neural network study. *J Neurophysiol* 103:117–139.
23. Xing J, Andersen RA (2000) Memory activity of LIP neurons for sequential eye movements simulated with neural networks. *J Neurophysiol* 84:651–665.
24. Wang X, et al. (2016) Perisaccadic receptive field expansion in the lateral intraparietal area. *Neuron* 90:400–409.
25. Zanos TP, Mineault PJ, Guitton D, Pack CC (2016) Mechanisms of saccadic suppression in primate cortical area V4. *J Neurosci* 36:9227–9239.
26. Jensen O, Bonnefond M, VanRullen R (2012) An oscillatory mechanism for prioritizing salient unattended stimuli. *Trends Cogn Sci* 16:200–206.
27. Heiser LM, Colby CL (2006) Spatial updating in area LIP is independent of saccade direction. *J Neurophysiol* 95:2751–2767.
28. Mirpour K, Bisley JW (2012) Anticipatory remapping of attentional priority across the entire visual field. *J Neurosci* 32:16449–16457.
29. Morris AP, Kubischik M, Hoffmann K-P, Krekelberg B, Bremmer F (2012) Dynamics of eye-position signals in the dorsal visual system. *Curr Biol* 22:173–179.
30. Cicchini GM, Binda P, Burr DC, Morrone MC (2013) Transient spatiotopic integration across saccadic eye movements mediates visual stability. *J Neurophysiol* 109:1117–1125.
31. Binda P, Cicchini GM, Burr DC, Morrone MC (2009) Spatiotemporal distortions of visual perception at the time of saccades. *J Neurosci* 29:13147–13157.
32. Umeno MM, Goldberg ME (2001) Spatial processing in the monkey frontal eye field. II. Memory responses. *J Neurophysiol* 86:2344–2352.
33. Inaba N, Kawano K (2014) Neurons in cortical area MST remap the memory trace of visual motion across saccadic eye movements. *Proc Natl Acad Sci USA* 111:7825–7830.
34. Hamker FH, Zirnsak M, Calow D, Lappe M (2008) The peri-saccadic perception of objects and space. *PLoS Comput Biol* 4:e31.
35. Duhamel JR, Bremmer F, Ben Hamed S, Graf W (1997) Spatial invariance of visual receptive fields in parietal cortex neurons. *Nature* 389:845–848.
36. Başar E, Schürmann M, Başar-Eroglu C, Karakaş S (1997) Alpha oscillations in brain functioning: An integrative theory. *Int J Psychophysiol* 26:5–29.
37. Berman RA, Wurtz RH (2011) Signals conveyed in the pulvinar pathway from superior colliculus to cortical area MT. *J Neurosci* 31:373–384.
38. Yao T, Treue S, Krishna BS (2016) An attention-sensitive memory trace in macaque MT following saccadic eye movements. *PLoS Biol* 14:e1002390.
39. Michalareas G, et al. (2016) Alpha-beta and gamma rhythms subserve feedback and feedforward influences among human visual cortical areas. *Neuron* 89:384–397.
40. Palva S, Palva JM (2011) Functional roles of alpha-band phase synchronization in local and large-scale cortical networks. *Front Psychol* 2:204.
41. von Stein A, Chiang C, König P (2000) Top-down processing mediated by interareal synchronization. *Proc Natl Acad Sci USA* 97:14748–14753.
42. Rohenkohl G, Nobre AC (2011) α oscillations related to anticipatory attention follow temporal expectations. *J Neurosci* 31:14076–14084.
43. Zanos TP, Mineault PJ, Pack CC (2011) Removal of spurious correlations between spikes and local field potentials. *J Neurophysiol* 105:474–486.

Supporting Information

Neupane et al. 10.1073/pnas.1701672114

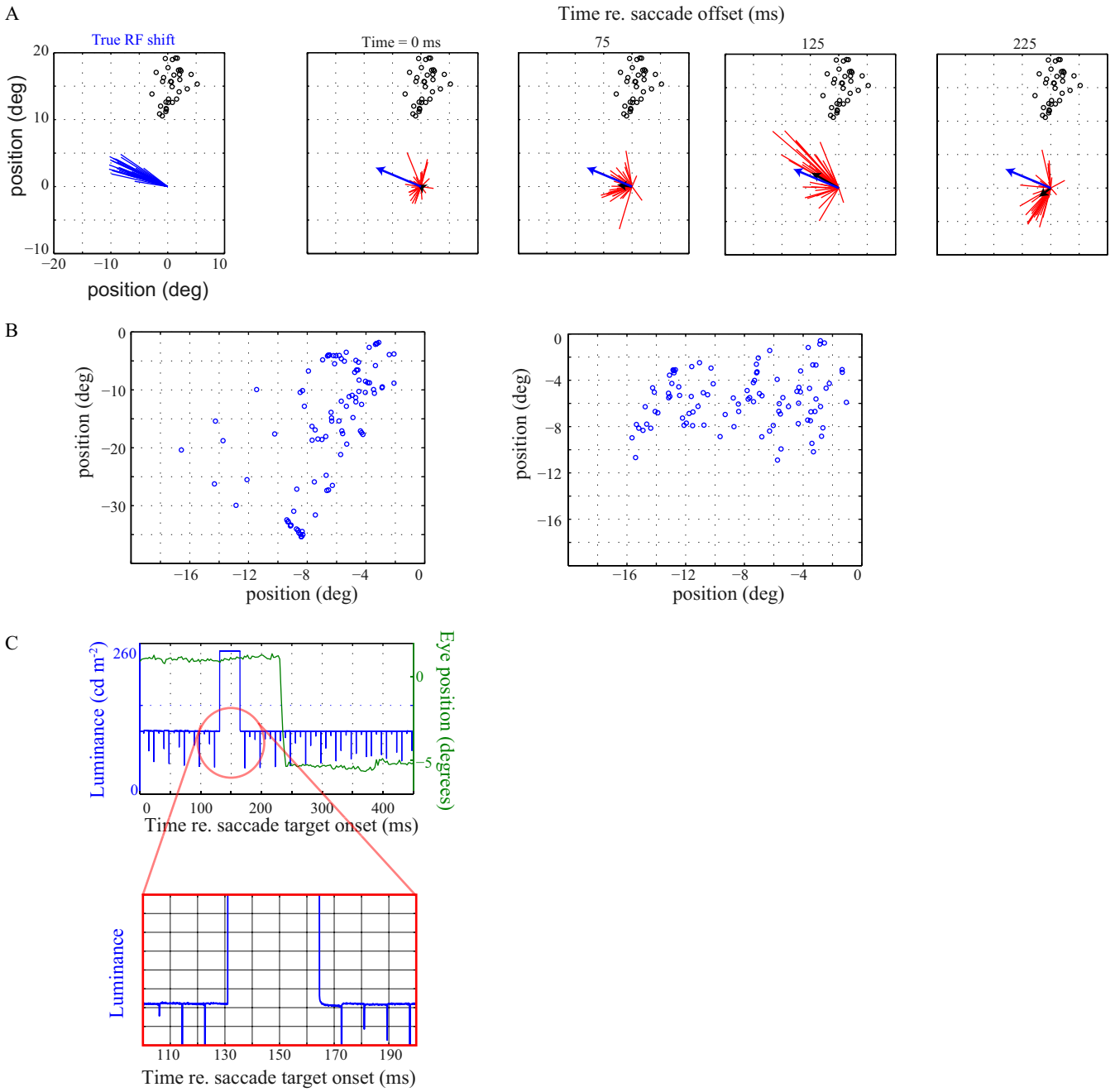

Fig. S1. Example of remapping in a population of V4 neurons. (*A*, *Left*) True receptive field (RF) shift vectors (obtained by joining RF centers measured 75 ms after P1 and P3 onset) of a population of 32 neurons, for oblique saccades in monkey P. The center of each P1 RF has been mapped to the origin of the plot. (*A*, *Right*) Observed remapping vectors of the population of cells at different times relative to saccade offset. Here, each red line indicates the displacement of one P2 RF from its corresponding P1 RF. The blue arrows represent the average true RF shift. The black arrows indicate the mean of the observed remapping vectors of the population. The small black circles represent the saccade target position relative to each current field. At early time points, the remapping vector length (mean amplitude of 2.1°) was less than the true shift (mean amplitude of 8.5°; $P < 0.001$, two-sample t test). At 125 ms after saccade offset, the mean remapping vector was 6.14°, which was not statistically different from the true shift ($P > 0.4$, two-sample t test). At the same time point, the angle of the remapping vector was significantly tuned to a mean value of 159° ($P < 0.001$, Rayleigh nonuniformity test), which was not different from the true shift angle of 160° [$F(1,62) = 0.029$, $P = 0.865$; Williamson–Watson two-sample test], indicating RF shifts toward the future field. deg, degree; re., relative to. (*B*) Retinotopies obtained from the array implant in monkey N (*Left*) and monkey P (*Right*). Each blue circle represents the center of an LFP RF. (*C*) Single-trial example of the photodiode recording of the P2 probe onset relative to the saccade (*Top*) and zoomed-in version of the same plot (*Bottom*) to show the luminance decay.

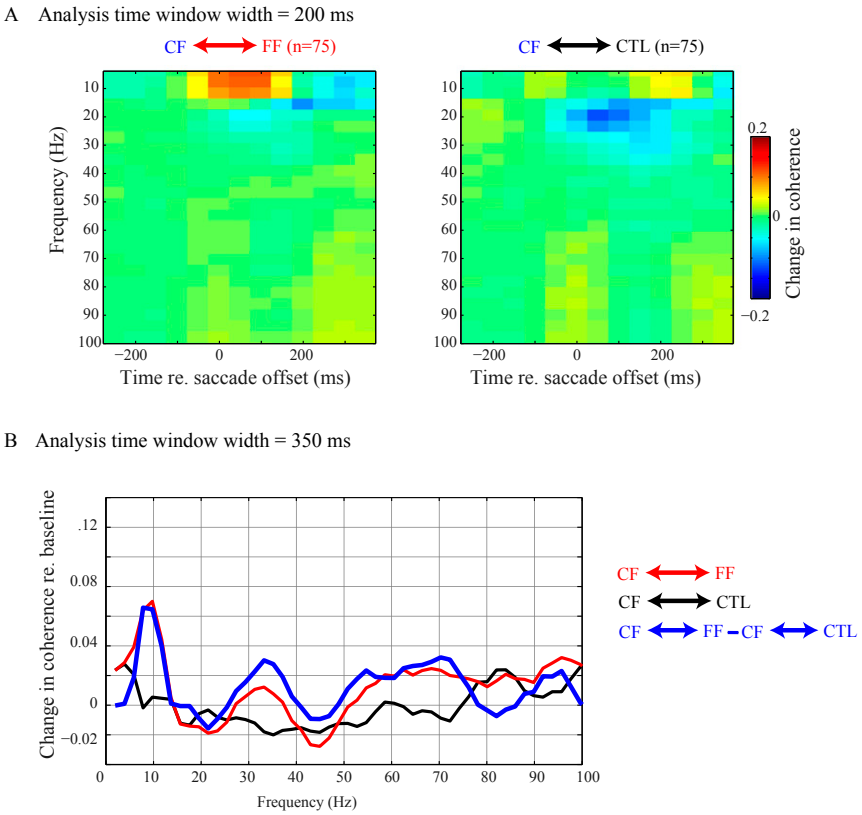

Fig. S2. (*A*) Average coherence spectrograms for 75 current-future field (*Left*) and current field-control (*Right*) pairs for horizontal saccades, with coherence calculated in a sliding 200-ms time window. CF, current field; CTL control; FF, future field. (*B*) Perisaccadic differences (blue) in coherence across frequencies between the current-future field pair (red) and current-control field pair (black) shown separately (same example pair as in Fig. 2*D*). Coherence is calculated in the 350-ms time window indicated in Fig. 2*C*.

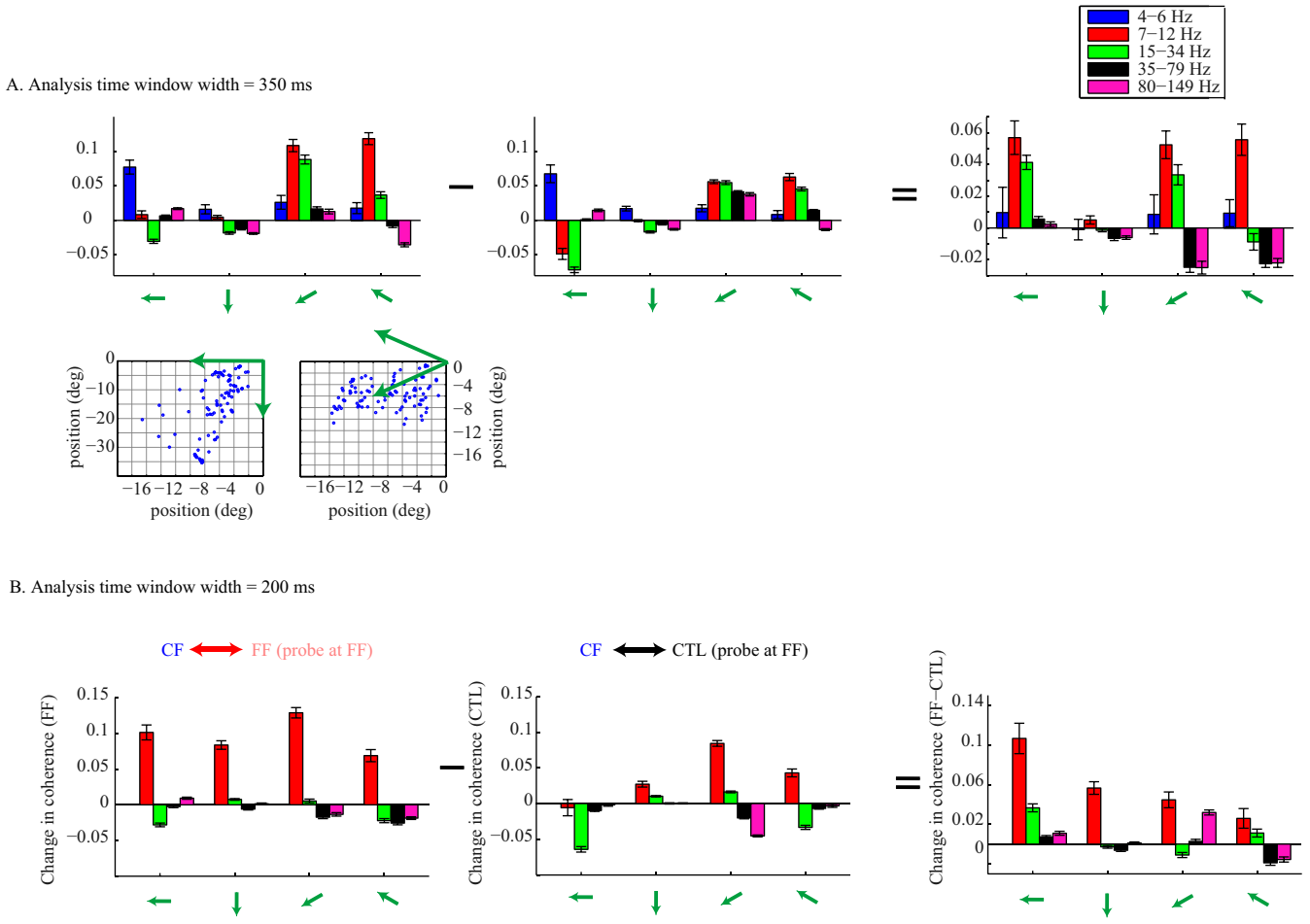

Fig. S3. (*A*, *Upper*) Mean coherence changes for current-future field pairs (*Left*), current field-control pairs (*Center*), and the difference between the two (*Right*) for standard frequency bands, shown separately for four saccade vectors. The time window of coherence calculation was 350 ms. (*A*, *Bottom*) Retinotopies of the two monkeys with superimposed saccade vectors. (*B*) Same as in *A*, but with a shorter time window (200 ms) for the coherence calculation.

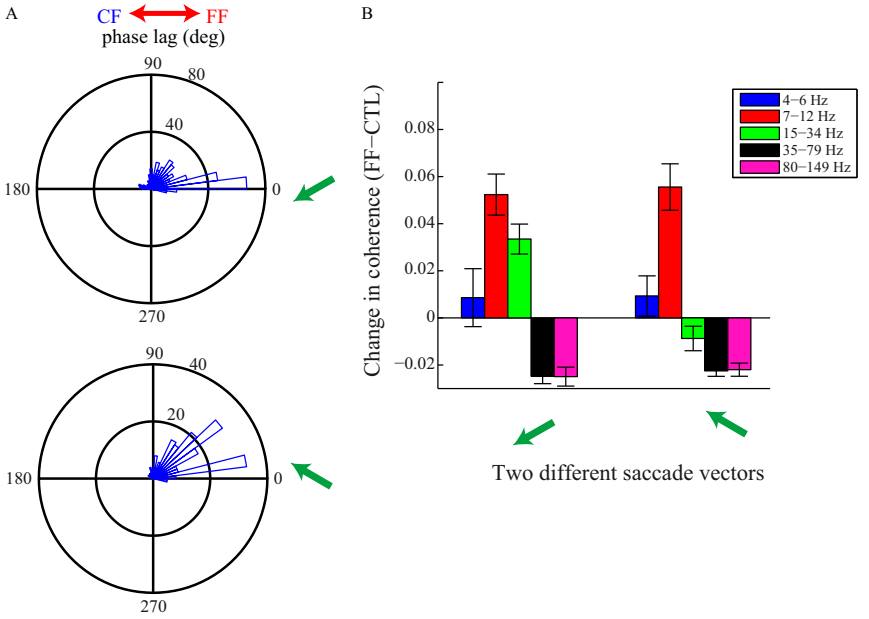

Fig. S4. Properties of perisaccadic coherence changes in monkey P. (*A*) Phase difference between alpha oscillations at the FF and CF sites for two different saccade vectors (green arrows). (*B*) Coherence changes relative to the presaccadic baseline across different frequency bands for the two saccade vectors.

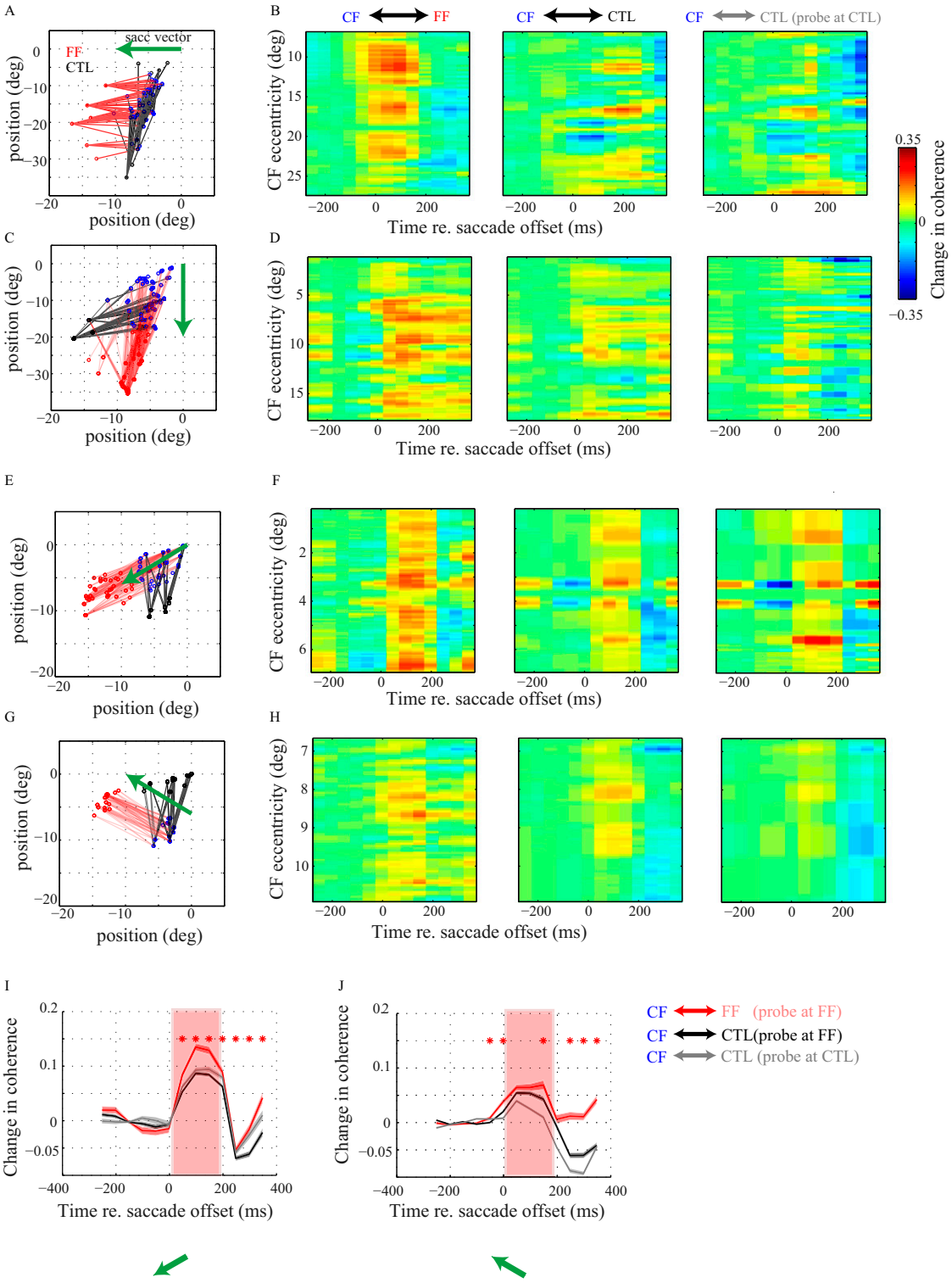

Fig. S5. Dependence of alpha coherence on saccade vector, receptive field location, and time. (*A*) Arrangement of current-future field electrode pairs (red) and current field-control pairs (black) for a 10° leftward saccade (green arrow). sacc, saccade. (*B*) Alpha coherence as a function of time (*x* axis) and current field eccentricity (*y* axis) for current-future field pairs (*Left*), current field-control pairs (*Center*), and current field-control pairs when probes were flashed at control field sites (*Right*). (*C* and *D*) As for *A* and *B*, but for a 20° vertical saccade. (*E*–*H*) As for *A* and *B*, but for oblique saccades in monkey P. (*I* and *J*) Timing of perisaccadic changes in alpha coherence for two different oblique saccades and for current-future field pairs (red), current-control field pairs (black), and current field-control pairs when probes were flashed in control field sites (gray). The shaded region represents the SEM, and asterisks represent statistically significant differences ($P < 0.05$, paired *t* test; $n = 151$ for *I* and $n = 71$ for *J*).

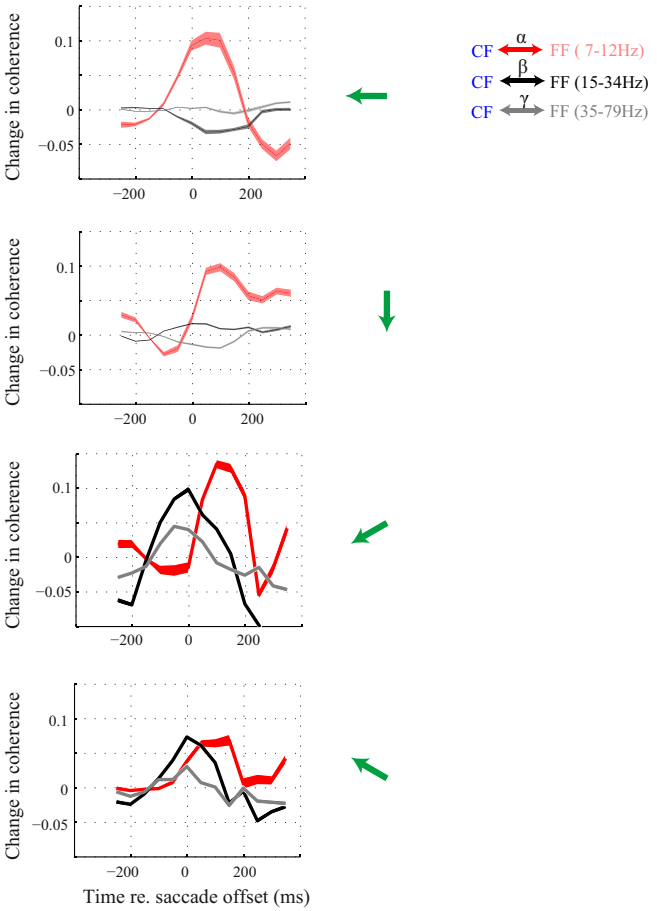

Fig. S6. Mean coherence change, relative to the presaccadic baseline, for current-future field pairs in the beta (black) and gamma (gray) bands superimposed on the mean coherence change in the alpha (red) band for four saccade vectors.

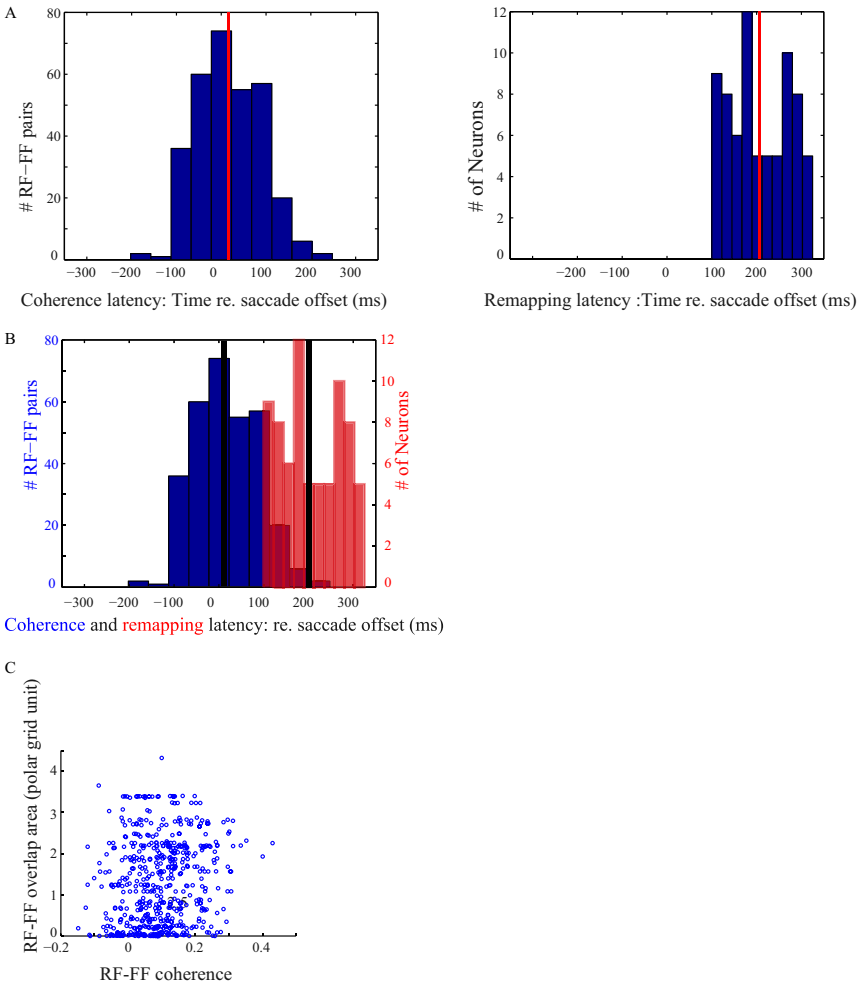

Fig. S7. (*A*, *Left*) Distribution of RF-FF coherence latency relative to the saccade offset (n = 313 pairs). (*A*, *Right*) Distribution of latency relative to saccade offset of the response to probes flashed at the future field (n = 71 neurons). (*B*) Histograms of coherence latency (blue) and remapping latency (red), superimposed. (*C*) Scatter plot of peak coherence between RF-FF pairs across all of the four saccade vectors against RF overlap of the corresponding RF-FF pairs.

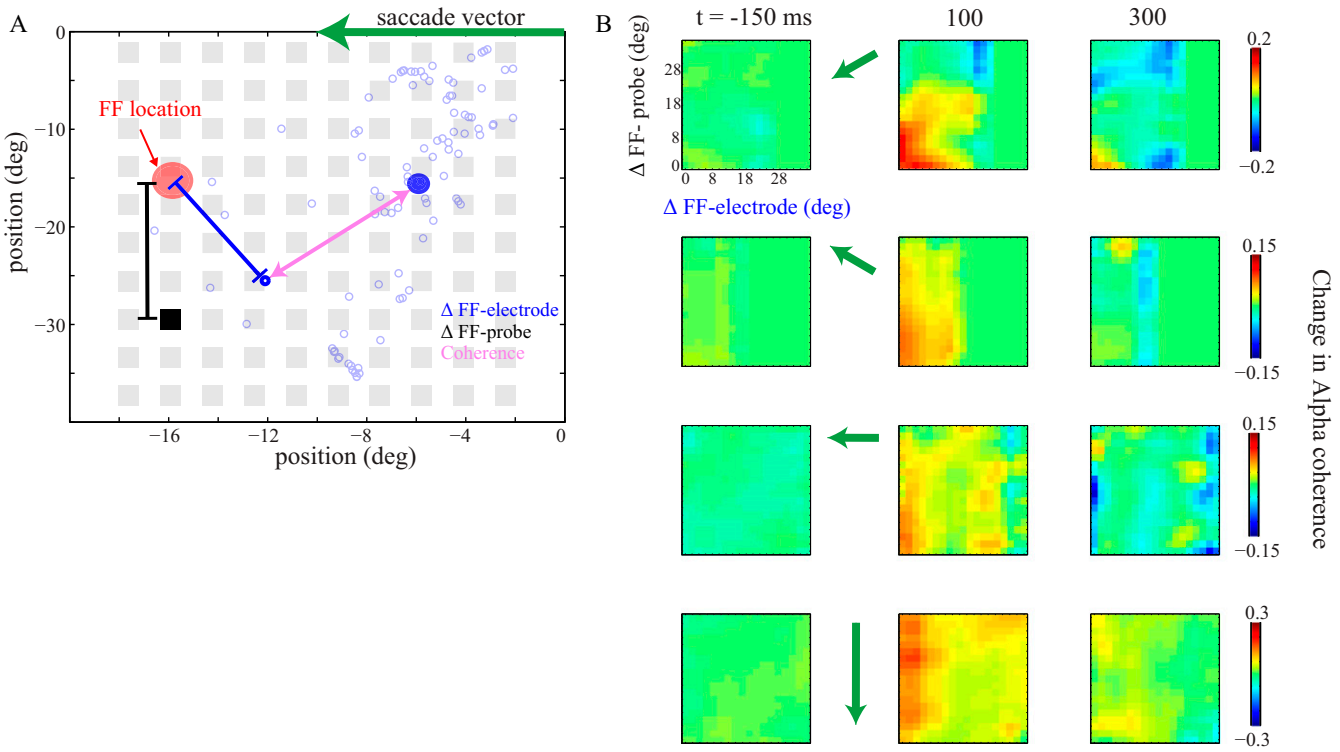

Fig. S8. Dependence of alpha coherence on probe position and receptive field location. (*A*) For each current field electrode (solid blue dot), we defined a FF location (red circle). For each trial, we considered the distance from this FF location to both the probe location (black square) and another electrode's receptive field center (small blue dot). We then measured coherence between this other electrode and the current field electrode (purple arrow). This procedure was repeated for all electrode pairs and all probe positions, and the results were averaged across current field positions. (*B*) Each panel summarizes alpha coherence across all combinations of probe distance and receptive field distance from the FF center. (*Center*) Alpha coherence is strongest at 100 ms after the saccade. Although there is some variability, alpha coherence between the current field electrode and another electrode is generally strongest when both the probe and the receptive field are near the FF.